Curvature-induced magnetization in a CrI_3 bilayer: Flexomagnetic effect enhancement in van der Waals antiferromagnets

Lei Qiao,[1] Jan Sladek,[2] Vladimir Sladek,[2] Alexey S. Kaminskiy,[3,4] Alexander P. Pyatakov,[3,4,*] and Wei Ren[1,5,†]

[1]*Physics Department, International Center of Quantum and Molecular Structures, Materials Genome Institute, State Key Laboratory of Advanced Special Steel, Shanghai Key Laboratory of High Temperature Superconductors, Shanghai University, Shanghai 200444, China*

[2]*Institute of Construction and Architecture, Slovak Academy of Sciences, 84503 Bratislava, Slovakia*

[3]*Physical Faculty, Lomonosov Moscow State University, 119991 Moscow, Russia*

[4]*MIREA - Russian Technological University, 119454 Moscow, Russia*

[5]*Zhejiang Laboratory, Hangzhou 311100, China*

(Received 17 July 2023; revised 5 December 2023; accepted 8 December 2023; published 11 January 2024)

The bilayer of CrI_3 is a prototypical van der Waals (vdW) 2D antiferromagnetic material with magnetoelectric effect. It is not generally known, however, that for symmetry reasons the flexomagnetic effect, i.e., the strain gradient-induced magnetization, is also possible in this system. In the present paper, based on the first-principle calculations, we estimate the flexomagnetic effect to be $200\,\mu_B \cdot$ Å, which is two orders of magnitude higher than it was predicted for the referent antiperovskite flexomagnetic material Mn_3GaN. The two major factors of flexomagnetic effect enhancement related to the peculiarities of antiferromagnetic structure of vdW magnets are revealed: the strain-dependent ferromagnetic coupling in each layer, and large interlayer distance separating antiferromagnetically coupled ions. Since 2D systems are naturally prone to mechanical deformation, the emerging field of flexomagnetism is of special interest for application in vdW spintronics, and straintronics in particular.

DOI: 10.1103/PhysRevB.109.014410

I. INTRODUCTION

Since the first report on graphene isolation, the class of two-dimensional (2D) materials has expanded tremendously: it includes now not only graphene derivatives (like graphane, graphone, graphyne, etc.) but also other types of van der Waals (vdW) materials including monolayers and bilayers of transition-metal dichalcogenides [1] and dihalides [2]. Some of these compounds have been recently discovered to demonstrate 2D magnetic ordering [3,4]. Since 2D materials are naturally prone to mechanical deformation, the study of cross-correlation effects between lattice, electronic, and magnetic subsystems is critical for straintronics, an emergent branch of electronics related to the strain-induced effects [5]. The advent of 2D magnets can bridge the gap between the two concepts of the straintronics of magnets [6] and the straintronics of vdW materials [7,8].

The flexural deformation (bending) characterized by strain gradient induces the electric polarization in the crystal, by the effect known as the flexoelectric one. In analogy to flexoelectricity the *flexomagnetic* effect, i.e., the strain gradient-induced magnetization was theoretically predicted [9,10] and experimentally found [11,12]. In 2D magnetic materials the flexorelated phenomena in spin subsystem of crystal have only very recently attracted attention of the researchers: the flexomagnetoelectric coupling in MoS_2 [13] and curvature-induced spin cycloid ordering in CrI_3 [14,15] were predicted by *ab initio* calculations; the flexomagnetic phase transition from antiferromagnetic to ferromagnetic order in rippled Heusler membranes was observed [16].

In this paper the CrI_3 bilayer is proposed as a material with a pronounced flexomagnetic effect, i.e., the magnetization linearly proportional to the strain gradient. In this way the flexomagnetic effect in a bilayer strikingly differs from curvature-induced magnetism in a monolayer analyzed in Refs. [14,15] both in phenomenology (linear vs nonlinear steplike curvature dependence) and in microscopic mechanisms (symmetrical Heisenberg-type exchange vs antisymmetrical Dzyaloshinskii-Moriya-like interaction). Flexomagnetic coefficients are obtained by fitting the density-functional theory (DFT) simulation with the analytical solution for a simple problem involving the gradient theory. The obtained value of flexomagnetic effect in a vdW bilayer is two orders of magnitude larger than the analogous effect in an antiperovskite [10] and other bulk materials.

II. STRUCTURE AND SYMMETRY

In a monolayer of CrI_3 the Cr atoms form a honeycomb structure as seen in Fig. 1(a). CrI_3 has two stacking styles, AB′ stacking (C_{2h} point group) with antiferromagnetic (AFM) interlayer interaction and AB stacking (S_6 point group) with ferromagnetic (FM) interlayer interaction; here we choose AB′ stacking [17]. The layer-dependent magnetic ordering was observed in this material [3]: ferromagnetism in the monolayer, antiferromagnetism in the bilayer [Fig. 1(b)], and nonvanishing magnetization in the trilayer, etc. The Cr atoms in every layer of multilayer are ferromagnetically coupled,

*pyatakov@physics.msu.ru
†renwei@shu.edu.cn

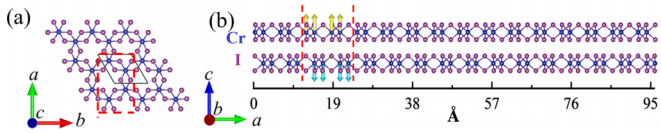

FIG. 1. (a) The top view of CrI_3 monolayer. (b) The cross section of CrI_3 undeformed bilayer. Blue and purple spheres are Cr and I atoms, respectively. The red dashed lines indicate the unit cell. The magnetic moments of Cr ions are shown in the unit cell with upward and downward arrows.

while the interlayer exchange is an antiferromagnetic one. CrI_3 bilayer is an antiferromagnet demonstrating linear magnetoelectric effect [18]; in other words, the symmetry of antiferromagnetic order parameter L allows $E_iH_jL_k$-type invariant combinations, and the contribution to the free energy of $F_{ME} = -\alpha_{ijk}E_iH_jL_k$, where E_i and H_j are the components of electric and magnetic fields, respectively. The existence of this invariant implies the magnetization linear with respect to the electric field: $M_j = -\frac{\partial F_{ME}}{\partial H_j} = \alpha_{ijk}E_iL_k$.

Since the strain gradient with respect to basic symmetry elements of space- and time inversion is an analog of electric field, then the magnetization proportional to the strain gradient, i.e., flexomagnetic effect, is possible. To investigate the exact structure of the flexomagnetic tensor let us consider the thermodynamic terms related to magnetic and mechanical subsystems in more detail.

III. TENSOR OF FLEXOMAGNETIC EFFECT AND FLEXOMAGNETIC COEFFICIENTS

The flexomagnetism can be phenomenologically described by incorporating additional strain-gradient terms into the expression for the thermodynamic potential. Then, the free-energy density for a piezomagnetic solid can be written as [10]

$$F = \tfrac{1}{2}c_{ijkl}\varepsilon_{ij}\varepsilon_{kl} - \tfrac{1}{2}\gamma_{ij}H_iH_j + \tfrac{1}{2}g_{jklmni}\eta_{jkl}\eta_{mni} - \xi_{ijkl}H_i\eta_{jkl}, \tag{1}$$

where H is a magnetic field, tensor γ components are the second-order magnetic permeabilities, c stands for the fourth-order elastic tensor, and ξ is the flexomagnetic effect tensor. The higher-order elastic coefficients corresponding to the strain-gradient η are denoted by g. No piezomagnetic properties are considered.

The linear strain tensor ε_{ij} is defined as

$$\varepsilon_{ij} = \tfrac{1}{2}(u_{i,j} + u_{j,i}), \tag{2}$$

where u_i is the displacement, the index after comma stands for spatial derivative component, and the stationary magnetic field H_i is expressed as the negative gradient of the magnetic potential. The strain-gradient tensor η is defined as

$$\eta_{ijk} = \varepsilon_{ij,k} = \tfrac{1}{2}(u_{i,jk} + u_{j,ik}). \tag{3}$$

The constitutive equations can be obtained from the free-energy density expression (1):

$$\sigma_{ij} = \frac{\partial F}{\partial \varepsilon_{ij}} = c_{ijkl}\varepsilon_{kl}, \quad \tau_{jkl} = \frac{\partial F}{\partial \eta_{jkl}} = -\xi_{ijkl}H_i + g_{jklmni}\eta_{mni},$$
$$B_i = -\frac{\partial F}{\partial H_i} = \gamma_{ij}H_j + \xi_{ijkl}\eta_{jkl}, \tag{4}$$

where σ_{ij}, B_i, and τ_{jkl} are the stress tensor, magnetic induction, and higher-order stress tensor, respectively. See Supplemental Material [19] for the matrix form of Eq. (4) represented by Lekhnitskii's notation [20].

To take into account the material microstructure in the phenomenological theory, the internal-length material parameter l has been introduced [21,22]. In the simplified model, the higher-order elastic coefficients g_{jklmni} can be expressed in terms of the conventional elastic stiffness coefficients c_{klmn} and this material parameter: $g_{jklmni} = l^2 c_{jkmn}\delta_{li}$, with δ_{li} being the Kronecker delta. Then, besides the classical material coefficients, the microlength-scale parameter is the additional material characteristic in the higher-grade continuum theory.

Two independent coefficients ξ_1 and ξ_2 are introduced for the flexomagnetic tensor ξ_{ijkl}:

$$\xi_{ijkl} = \xi_1\delta_{jk}\delta_{il} + \xi_2(\delta_{ij}\delta_{kl} + \delta_{ik}\delta_{jl}). \tag{5}$$

In the framework of this theory the free-energy density has the following form:

$$F = \frac{1}{2}c_{ijkl}\varepsilon_{ij}\varepsilon_{kl} - \frac{1}{2}\gamma_{ij}H_iH_j + \frac{l^2}{2}c_{jkmn}\eta_{jkl}\eta_{mnl} - \xi_1H_i\eta_{kki} - 2\xi_2H_i\eta_{ikk}. \tag{6}$$

Governing equations are obtained from the principle of virtual work, $\delta F - \delta W = 0$:

$$\varepsilon_{ij,j}(\mathbf{X}) - \tau_{ijk,jk}(\mathbf{X}) = 0, \quad B_{i,i}(\mathbf{X}) = 0. \tag{7}$$

Let us consider a boundary value condition for the rectangle domain $L \times d$, where L is the length of the film fragment under consideration and d is the thickness of the 2D material layer. The displacements are assumed as

$$u_1 = 0, \quad u_3 = a_1x^2 + a_2z^2, \tag{8}$$

where a_1 and a_2 are coefficients corresponding to the strain gradient. Here the coordinate system (x, z) corresponds to (x_1, x_3).

It can be shown from the governing equation (7) (for details, see Supplemental Material [19]) that the strain-gradient coefficients and that for magnetic induction are related by the following equations:

$$\frac{a_1}{a_2} = -\frac{c_{33}}{c_{44}}, \tag{9}$$

$$B_3 = 2(\xi_1 + 2\xi_2)a_2 + 2\xi_2a_1 = 2a_2\left[\xi_1 + \left(2 - \frac{c_{33}}{c_{44}}\right)\xi_2\right]. \tag{10}$$

Specification of coefficients by (9) guarantees not only satisfaction of continuum-theory governing equations, but results also into the complete set of boundary conditions in the classical continuum theory for condition A (see the boundary value condition A section in the Supplemental Material [19]).

In order to obtain the second equation for unknown coefficients ξ_1 and ξ_2, another boundary condition should be considered [Fig. 2(b)]:

$$u_1 = a_3x^2 + a_4z^2, \quad u_3 = 0, \tag{11}$$

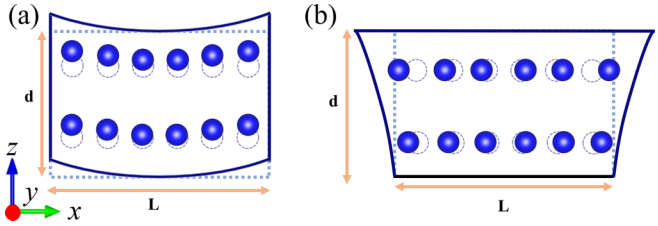

FIG. 2. Schematic diagram of two deformation modes. Symmetric boundary conditions for (a) a simple patch condition A: $u_3 = a_1x^2 + a_2z^2$, where $a_1 = -(c_{33}/c_{44})a_2$, and (b) a simple patch condition B: $u_1 = a_3x^2 + a_4z^2$, where $a_3 = -(c_{44}/c_{11})a_4$. Dashed and solid lines indicate the lattice box and the position of atoms before and after deformation.

From the governing equations we get relations for strain gradients:

$$a_3 = -\frac{c_{44}}{c_{11}}a_1, \tag{12}$$

and the magnetic induction:

$$B_1 = 2(\xi_1 + 2\xi_2)a_3 + 2\xi_2 a_4 = 2a_4\left[\xi_2 - \frac{c_{44}}{c_{11}}(\xi_1 + 2\xi_2)\right]. \tag{13}$$

Finally, we have two expressions for magnetic inductions (10) and (13) with two unknown flexomagnetic coefficients ξ_1 and ξ_2. If both values B_1 and B_3 are obtained from DFT calculations, it is easy to get both unknown flexomagnetic parameters.

IV. COMPUTATIONAL DETAILS

DFT simulations were performed within the generalized gradient approximation [23] in the form proposed by Perdew-Burke-Ernzerhof, as implemented in the Vienna *Ab initio* Simulation Package (VASP) [24]. The projector augmented-wave pseudopotentials [25,26] were used. For all the calculations, we chose the energy cutoff to be 500 eV, and an additional effective Hubbard $U_{\text{eff}} = 3$ eV for Cr $3d$ orbitals to deal with the self-interaction error [27]; the convergence criterion of the total energy was set to less than 10^{-6} eV. We chose the high-temperature phase-stacking structure, and transformed the unit cell as shown in Fig. 1, optimized to have the lattice parameters of $a = 11.97$ Å and $b = 6.91$ Å. To simulate the experimental condition, we used a nanoribbon composed of $8\times1\times1$ supercell while adding a vacuum larger than 15 Å in the a direction. Thus, the final structure dimensions are $a = 119.78$ Å, $b = 6.91$ Å, and $c = 41.39$ Å with $\alpha = \beta = \gamma = 90^\circ$. When the bilayer inside has no strain gradient, the thickness of monolayer and the vdW gap are 3.2 and 3.5 Å, respectively, which gives $2\times3.2 + 3.5 = 9.9$ Å thickness of the bilayer. The system contains 64 Cr and 192 I atoms. The $1\times5\times1$ Γ-centered k-grid samplings [28] were adopted for the system. For the mechanical properties, we used the energy-strain method to calculate the elastic constants, generating input files based on VASPKIT [29] with strains ranging from −1 to 1% and fitting the energy to obtain the elastic constants of the system.

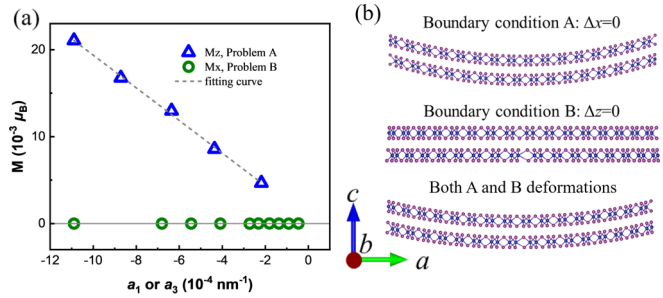

FIG. 3. The calculated flexomagnetic effect: (a) the magnetization dependence on the strain-gradient parameters a_1 and a_3 along x axis for boundary conditions A and B, respectively. (b) The configurations for the boundary conditions A and B, as well as the superposition of A and B deformations (the deformations are exaggerated by 10 times for illustrative purposes).

V. RESULTS

As analyzed in the model, we moved the atoms in the supercell to simulate three situations; again, the displacements were $u_1 = 0, u_3 = a_1(x^2 + \frac{z^2 c_{44}}{c_{33}})$ for boundary condition A, while $u_1 = a_3(x^2 + \frac{z^2 c_{11}}{c_{44}}), u_3 = 0$ for boundary condition B. The bend deformation means that both boundary conditions A and B exist, and note that $a_1 = a_3$ for bend deformation. Figure 3(b) shows the structures for the three conditions. To make the structural features more obvious, the displacement distance of atoms is exaggerated in the figure, and the negative value of strain gradient means that the surface of the bilayer is concave.

First, we calculated the elastic constant of the boundary conditions A and B. As described in the Supplemental Material [19], we already had the representation of the elastic constant matrix of the orthotropic material; these values in the matrix could be obtained from the fit of the direction-specific strain-energy curve. The energy-strain curves of boundary conditions A and B, shown in Fig. S1, give the ratio for the elastic constant in Table SI: $\frac{c_{33}}{c_{44}} \approx 1.8$ and $\frac{c_{44}}{c_{11}} \approx 0.42$. Since c_{11} and c_{33} represent the deformation along the x direction and z direction, respectively, the c_{44} represents the deformation along the yz plane; it can be predicted that the order of influence of the interlayer distance on the elastic constant is $c_{33} > c_{44} > c_{11}$, and further affects the ratio of elastic constants. The data in Tables SII and SIII prove the above analysis.

The dependence of strain gradient-induced magnetic moments of CrI_3 bilayer per formula unit corresponding to Eqs. (10) and (13) are shown in Fig. 3(a). Note that the magnetic moment of the end Cr atoms increases substantially due to the formation of dangling bonds by the unpaired electrons [it is clear to find the Cr's position in Fig. 1(b)]. For a more accurate description of the total magnetic moment, we do not consider the contribution of dangling bonds in the total magnetic moment, and as an example we show the effect of dangling bonds in Fig. S2.

Taking into account the data of Fig. 3 one can see that the flexomagnetic magnetization along the x axis (the boundary condition B) is negligible with respect to the one along the normal to the plane. This result agrees with the Curie principle: the symmetry of the crystal structure (Fig. 1) and

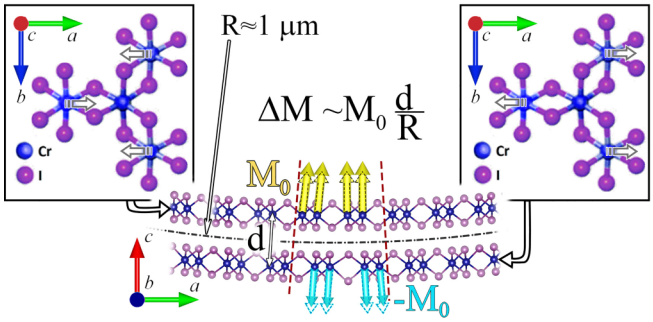

FIG. 4. On the mechanisms of flexomagnetic effect enhancement: M_0 is the moment of a single ion in the antiferromagnetic sublattice, d is the distance between the middle lines of the top and bottom CrI_3 layers, R is the curvature radius that is inversely proportional to a strain gradient a_2 along z axis. The top views of relative displacements of Cr ions in the top and the bottom layers are shown in the insets. The dashed lines show the boundaries of the unit cell. The dashed-dotted line shows the middle line of the bilayer. The dotted arrows correspond to the initial magnetic moments of atoms M_0: one can see the increment of magnetization in the top layer and the decrement in the bottom one that results in magnetization decompensation ΔM. The curvature of the layers is exaggerated for illustrative purposes.

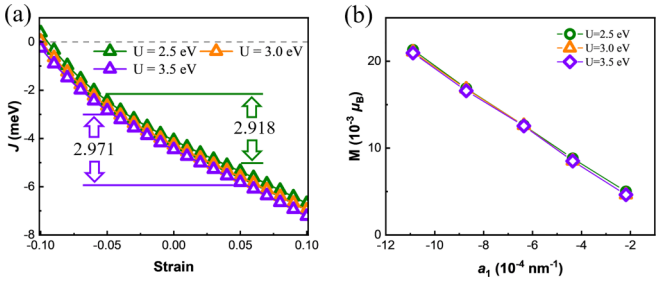

FIG. 5. We chose the Hubbard U parameters of 2.5, 3.0, and 3.5 eV to calculate (a) the modulation of the nearest Cr-Cr neighbor exchange parameters vs strain $(a - a_0)/a_0$ and (b) the total magnetic moment vs strain-gradient parameter a_1.

symmetry of the "cause" [the deformation, Fig. 2(b)] do not single out any preferential direction in the plane of the bilayer.

Taking into account that B_1 is negligibly small [Eq. (13)], one can estimate the ratio of flexomagnetic constants $\xi_2/\xi_1 \approx 4.5$. The values of flexomagnetic coefficients in accordance to Eq. (10) are $\xi_2 \approx 239\ \mu_0\mu_B \cdot$ Å and $\xi_1 \approx 53\ \mu_0\mu_B \cdot$ Å.

Substituting these values of the flexomagnetic coefficients into Eq. (10), we obtained that the strain gradient-induced magnetic moment along the normal to the plane was proportional to strain-gradient a_2 with the coefficient $200\,\mu_B \cdot$ Å that is about two orders of value larger than the analogous flexomagnetic effect in Mn_3GaN [10].

VI. DISCUSSION

To rationalize the obtained numerical results let us consider the vdW bilayer CrI_3 as a system of two oppositely magnetized layers playing the role of sublattices in a conventional antiferromagnet (Fig. 4). From the general arguments the flexomagnetic effect is proportional to the magnetic moment M_0 of a single ion in an antiferromagnetic sublattice and to the distance d between the pair of antiferromagnetically ordered ions. This distance in the vdW structure of CrI_3 bilayer (6.7 Å) is unusually large for antiferromagnet. The larger the space separation between antiferromagnetically coupled ions is, the more pronounced the difference in their crystalline environments in the presence of strain gradient is. This strain-induced difference in the sublattices' crystal structure results in the imbalance of their magnetizations, i.e., flexomagnetic effect.

When comparing CrI_3 bilayer with the referent flexomagnetic material Mn_3GaN one should consider that the magnetic moment of Cr ion $M_0 \sim 3\ \mu_B$ is somewhat bigger than $M_0 \sim 2\mu_B$ for Mn ion and that the antiferromagnetically coupled Cr ions are separated by the spacing $d = 7$ Å, while in antiperovskite unit cell of Mn_3GaN the distance between Mn ions belonging to different antiferromagnetic sublattices does not exceed 2 Å. However, these factors alone cannot explain two orders of magnitude increase of flexomagnetic effect in CrI_3 bilayer compared to Mn_3GaN.

Besides these purely geometrical arguments there are also the physical mechanisms of flexomagnetic effect enhancement: the strong dependence of exchange interaction on the distance between atoms (the vivid illustration is Ruderman-Kittel-Kasuya-Yosida interaction where even the sign of exchange integral changes with distance [16]) or the strain-induced modulation of Néel temperature [12]. Within the limits of our model the most probable reason for flexomagnetic effect enhancement is the strain-induced exchange modulation: in the top layer the ferromagnetically ordered Cr ions are closer to each other than in the relaxed state while in the bottom layer they move apart (Fig. 4, insets).

The value of intralayer exchange modulation induced by the strain can be estimated from Ref. [30]: in the linear approximation the tensile/compressive strain 0.1% corresponds to the reduction/increase of the exchange coupling by 0.5%. The effective exchange field for Cr ions in the compressed top layer is higher than in the stretched bottom layer, resulting in the decompensation of the sublattice magnetizations. To illustrate this in Fig. S3, the structures with different interlayer distance are calculated: the increase of the distance leads to the proportional uncompensated magnetic moment due to the change of strain difference in layers [Fig. S3(a)]. The change of interlayer distance alone (without corresponding change of strains in layers) basically has no effect on the total magnetic moment [Fig. S3(b)]. Proving the above analysis, we confirm that the noncanceled magnetic moment comes from the *different* strain degrees in the two layers of CrI_3.

The value of flexomagnetic effect $200\,\mu_B \cdot$ Å enables to detect it by highly sensitive single-spin magnetometry based on a nitrogen-vacancy center (NV center) [31]: if the curvature radius of the ripple is below 1000 Å (that is equivalent to the strain gradient higher than 10^{-3} Å^{-1}) the strain-induced moment per formula unit will be above $0.1\mu_B$. It should be noted that these curvature values are well below the ones for CrI_3 monolayer ($\sim$0.1 Å^{-1}) considered in Refs. [14,15], so the curvature-induced effects due to the spin-orbit interaction can be neglected here; see Fig. S4 in Supplemental Material [19] for the specific derivation [14,32]. In addition, it is observed in Fig. 5 that different Hubbard U parameters slightly

change the magnetic exchange parameters without changing the total magnetic moment much, since the total magnetic moment essentially comes from the difference in exchange parameter caused by different strains between the bilayers, and has nothing to do with the strength of the exchange parameter itself. At the same time, the difference in magnetic exchange parameters obtained by different U parameters is basically unchanged, such as the difference of magnetic exchange parameter between −5 and 5% strains calculated with U equals 2.5 and 3.5 eV in Fig. 5(a) is less than 2%, resulting in a total magnetic moment that is not related to the U parameter.

VII. CONCLUSION

Summarizing, the flexomagnetic effect in CrI_3 bilayer is the result of strain gradient-induced decompensation of antiferromagnetic sublattices and manifests itself on the rippled surface. As soon as the curvature radius of a ripple scales down to the range of hundreds of nanometers and below, the magnetic moment difference per formula unit reaches $0.1\mu_B$ that is within the range of single-spin NV-center magnetometry. The relatively large value of flexomagnetic effect in the bilayer CrI_3 is partly attributable to the large distance between the antiferromagnetically coupled ions in the vdW structure compared to the conventional antiferromagnets, but this geometrical factor alone cannot explain the two-order enhancement of flexomagnetic coefficient compared to antiperovskite Mn_3GaN. To gain insight into the origin of the enhancement the strain-induced ferromagnetic exchange modulation in each layer should be involved. The flexomagnetic effect provides a powerful knob to control magnetic properties of antiferomagnetically coupled vdW structures and is interesting for application in spintronics of 2D magnets and straintronics in particular.

ACKNOWLEDGMENTS

This work was supported by the National Natural Science Foundation of China (Grants No. 12074241, No. 12311530675, No. 11929401, and No. 52130204), the Russian Ministry of Science and Education (Project No. 075–15–2022–1131), the Science and Technology Commission of Shanghai Municipality (Grants No. 22XD1400900, No. 20501130600, No. 21JC1402600, and No. 21JC1402700), High Performance Computing Center, Shanghai University, and Key Research Project of Zhejiang Laboratory (Grant No. 2021PE0AC02). L.Q. acknowledges the support of China Scholarship Council. J.S. and V.S. acknowledge the support by the Slovak Science and Technology Assistance Agency registered under Grant No. APVV-18–0004, and the support by the Ministry of Education, Science, Research and Sport of the Slovak Republic under Grant No. VEGA-2/0061/20. A.P.P. and A.S.K. acknowledge the support of the Basis Foundation "Junior leader" program.

[1] N. Zibouche, A. Kuc, J. Musfeldt, and T. Heine, Transition-metal dichalcogenides for spintronic applications, Ann. Phys. **526**, 395 (2014).

[2] A. S. Botana and M. R. Norman, Electronic structure and magnetism of transition metal dihalides: Bulk to monolayer, Phys. Rev. Mater. **3**, 044001 (2019).

[3] B. Huang *et al.*, Layer-dependent ferromagnetism in a van der Waals crystal down to the monolayer limit, Nature (London) **546**, 270 (2017).

[4] X. Liu, A. P. Pyatakov, and W. Ren, Magnetoelectric coupling in multiferroic bilayer VS_2, Phys. Rev. Lett. **125**, 247601 (2020).

[5] A. Bukharaieva, A. Zvezdin, A. Piatakov, and K. Fetisov Yu, Straintronics: A new trend in micro- and nanoelectronics and materials science, Phys. Usp. **61**, 1175 (2018).

[6] K. Roy, S. Bandyopadhyay, and J. Atulasimha, Hybrid spintronics and straintronics: A magnetic technology for ultra low energy computing and signal processing, Appl. Phys. Lett. **99**, 063108 (2011).

[7] V. Atanasov and A. Saxena, Electronic properties of corrugated graphene: The Heisenberg principle and wormhole geometry in the solid state, J. Phys.: Condens. Matter **23**, 175301 (2011).

[8] F. Miao, S.-J. Liang, and B. Cheng, Straintronics with van der Waals materials, npj Quantum Mater. **6**, 59 (2021).

[9] E. A. Eliseev, A. N. Morozovska, M. D. Glinchuk, and R. Blinc, Spontaneous flexoelectric/flexomagnetic effect in nanoferroics, Phys. Rev. B **79**, 165433 (2009).

[10] P. Lukashev and R. F. Sabirianov, Flexomagnetic effect in frustrated triangular magnetic structures, Phys. Rev. B **82**, 094417 (2010).

[11] B. A. Belyaev, A. V. Izotov, P. N. Solovev, and N. M. Boev, Strain-gradient-induced unidirectional magnetic anisotropy in nanocrystalline thin permalloy films, Phys. Status Solidi RRL **14**, 1900467 (2020).

[12] P. Makushko *et al.*, Flexomagnetism and vertically graded Néel temperature of antiferromagnetic Cr_2O_3 thin films, Nat. Commun. **13**, 6745 (2022).

[13] Y. H. Shen, Y. X. Song, W. Y. Tong, X. W. Shen, S. J. Gong, and C. G. Duan, Giant flexomagnetoelectric effect in dilute magnetic monolayer, Adv. Theory Simul. **1**, 1800048 (2018).

[14] A. Edström, D. Amoroso, S. Picozzi, P. Barone, and M. Stengel, Curved magnetism in CrI_3, Phys. Rev. Lett. **128**, 177202 (2022).

[15] G. Qiu, Z. Li, K. Zhou, and Y. Cai, Flexomagnetic noncollinear state with a plumb line shape spin configuration in edged two-dimensional magnetic CrI_3, npj Quantum Mater. **8**, 15 (2023).

[16] D. Du, S. Manzo, C. Zhang, V. Saraswat, K. T. Genser, K. M. Rabe, P. M. Voyles, M. S. Arnold, and J. K. Kawasaki, Epitaxy, exfoliation, and strain-induced magnetism in rippled Heusler membranes, Nat. Commun. **12**, 2494 (2021).

[17] N. Ubrig, Z. Wang, J. Teyssier, T. Taniguchi, K. Watanabe, E. Giannini, A. F. Morpurgo, and M. Gibertini, Low-temperature monoclinic layer stacking in atomically thin CrI_3 crystals, 2D Mater. **7**, 015007 (2020).

[18] S. Jiang, J. Shan, and K. F. Mak, Electric-field switching of two-dimensional van der Waals magnets, Nat. Mater. **17**, 406 (2018).

[19] See Supplemental Material at http://link.aps.org/supplemental/10.1103/PhysRevB.109.014410 for the derivation of phenomenological approach to flexomagnetic coupling and more

detailed DFT results. The Supplemental Material also contains Refs. [14,20,32].

[20] S. G. Lekhnitskii, *Theory of Elasticity of an Anisotrophic Elastic Body* (Holden-Day, Moscow, 1963).

[21] I. M. Gitman, H. Askes, E. Kuhl, and E. C. Aifantis, Stress concentrations in fractured compact bone simulated with a special class of anisotropic gradient elasticity, Int. J. Solids Struct. **47**, 1099 (2010).

[22] S. T. Yaghoubi, S. M. Mousavi, and J. Paavola, Buckling of centrosymmetric anisotropic beam structures within strain gradient elasticity, Int. J. Solids Struct. **109**, 84 (2017).

[23] J. P. Perdew, K. Burke, and M. Ernzerhof, Generalized gradient approximation made simple, Phys. Rev. Lett. **77**, 3865 (1996).

[24] G. Kresse and J. Hafner, Ab initio molecular dynamics for liquid metals, Phys. Rev. B **47**, 558 (1993).

[25] P. E. Blöchl, Projector augmented-wave method, Phys. Rev. B **50**, 17953 (1994).

[26] G. Kresse and D. Joubert, From ultrasoft pseudopotentials to the projector augmented-wave method, Phys. Rev. B **59**, 1758 (1999).

[27] J. He, S. Ma, P. Lyu, and P. Nachtigall, Unusual Dirac half-metallicity with intrinsic ferromagnetism in vanadium trihalide monolayers, J. Mater. Chem. C **4**, 2518 (2016).

[28] H. J. Monkhorst and J. D. Pack, Special points for Brillouin-zone integrations, Phys. Rev. B **13**, 5188 (1976).

[29] V. Wang, N. Xu, J.-C. Liu, G. Tang, and W.-T. Geng, VASPKIT: A user-friendly interface facilitating high-throughput computing and analysis using VASP code, Comput. Phys. Commun. **267**, 108033 (2021).

[30] M. Pizzochero and O. V. Yazyev, Inducing magnetic phase transitions in monolayer CrI_3 via lattice deformations, J. Phys. Chem. C **124**, 7585 (2020).

[31] I. Gross *et al.*, Real-space imaging of non-collinear antiferromagnetic order with a single-spin magnetometer, Nature (London) **549**, 252 (2017).

[32] A. K. Zvezdin and A. P. Pyatakov, On the problem of coexistence of the weak ferromagnetism and the spin flexoelectricity in multiferroic bismuth ferrite, Europhys. Lett. **99**, 57003 (2012).